J. Appl. Comput. Mech., 6(SI) (2020) 1133-1140
DOI: 10.22055/JACM.2020.31423.1871

ISSN: 2383-4536
jacm.scu.ac.ir

Shahid Chamran University of Ahvaz

Journal of Applied and Computational Mechanics

Research Paper

Numerical Calculation of an Air Centrifugal Separator Based on the SARC Turbulence Model

Madaliev Murodil Erkinjon son

Institute of Mechanics and Earthquake Engineering M.T. Urazbaev, Academy of Sciences of the Republic of Uzbekistan, Tashkent, Uzbekistan

Received October 17 2019; Revised March 01 2020; Accepted for publication March 01 2020.
Corresponding author: M. Murodil (Madaliev.me2019@mail.ru)

Abstract: The numerical results of mathematical modeling of a two-phase swirling turbulent flow in the separation zone of a centrifugal apparatus are presented. The motion of the carrier gas flow was modeled using the averaged Navier-Stokes equations, for the closure of which the well-known turbulence model by Schur and Spalart was used, the amendment to the Spalart-Allmaras SARC model. Based on the obtained field of averaged velocities of the carrier medium, taking into account turbulent diffusion. The article compares the results taking into account the influence of the solid phase on the dynamics of the air environment and without taking it into account with experimental data.

Keywords: Reynolds-averaged Navier-Stokes equations, SARC model, Centrifugal air separator, Current function, Vorticity, iteration, Eddy viscosity, Sweep, Upper relaxation.

1. Introduction

In modern technological processes, swirling flows of gases and liquids are often found [1]. The formation of swirling flows occurs behind the wheels of hydroelectric turbines of a hydroelectric power station [2], in the wake of aircraft and propellers, as well as wind generators, etc. [3]. Cyclones, separators, vortex flowmeters - all of these devices use a swirl of the working fluid flow. Useful properties of swirling flows are widely used in the power industry; for example, they help to stabilize the flame in burner devices. However, swirling flows have not only positive features. In strongly swirling flows, the formation of unsteady structures, such as a precessing vortex core (PWC), often occurs. Low frequencies of the precession of the vortex core, formed, for example, behind the wheel of a hydroelectric turbine of a hydroelectric power station, can lead to resonance with the natural frequencies of the hydroelectric unit, which in turn will entail strong vibrations, which pose a serious danger to the entire structure of a hydroelectric power station. The formation of PWC in vortex combustion chambers can cause thermoacoustic resonance [4], which also results in strong vibrations and noise. In addition, it was found that PWC can affect the efficiency of vortex devices [5]. Despite many years of research on this phenomenon, at the moment, there is not enough information to construct a theory of PWC and, accordingly, to develop effective methods for controlling this phenomenon. For this reason, the study of the effect of PWC is still an urgent task [6].

Swirling flows can be accompanied by such non-stationary effects as the precession of the vortex core. In turn, large-scale pulsations caused by the precession of the vortex can lead to structural damage and reduce equipment reliability. Thus, for engineering calculations, turbulence models are required that accurately describe the averaged fields and large-scale pulsations of swirling flows. Widely used in engineering calculations, the k-ε and k-ω turbulence models poorly describe such flows. To improve the modeling of turbulent swirling flows, they are trying to modify existing RANS models (Reynolds-Averaged Navier-Stokes Equations - turbulence averaged by Reynolds equations). In [7], Schur and Spalart proposed an amendment to the Spalart-Allmaras (SA) model [8]. The new model, called SARC, was tested on a large number of swirling turbulent flows.

It is known that swirling flows are characterized by a strong curvature of streamlines, the appearance of recirculation zones, the location and dimensions of which depend to a large extent on twist intensity, and the configuration of the boundaries. In addition, such flows are turbulent. Therefore, their study requires the use of effective turbulence models. Recently, quite effective turbulence models have appeared [7, 9-10]. These methods were further modified for turbulent flows with a small swirl [11-12].

In this paper, we consider a three-dimensional turbulent flow in an air-centrifugal separator, which is an important link in the processes of separation and classification of particles, obtaining powders of the required quality. The efficiency of the processes involved in the separation of powders into coarse and fine fractions will depend on how the structure of the flow is organized inside the workspace. The undertaken numerical study aims to clarify the nature of the hydrodynamics of the swirling flow at different geometries. The scheme of the calculated area is shown in (Fig. 1).

Published online: May 15 2020

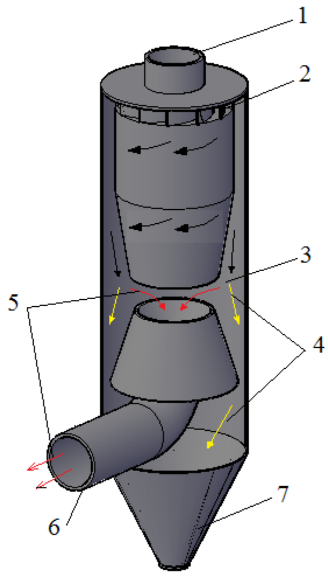

Fig. 1. Scheme of the calculated air-centrifugal separator.

2. Physical and Mathematical Formulations of the Problem

The source material together with the primary air, is supplied through the pipe 1 to the upper part of the separator. Using controlled shovels 2, a rotational movement is imparted to the airflow. Under the action of centrifugal inertia, the particles move to the outer cylindrical wall of the separator body and fall into classification zone 3 located between the cones and the walls (see Fig. 1). Large particles (yellow line) 4 due to their greater mass under the action of centrifugal force accumulate near the inner wall of the separator housing and by inertia fall into the hopper of the separator 7. Moreover, small particles (red line) 5 are entrained in air and carried out of the separator through the outlet pipe 6. Thus thus, the starting material is divided into two fractions. It is easy to understand that the effectiveness of such a separator is highly dependent on its geometry. Therefore, to find the optimal geometric parameters, the problem arises of modeling the kinematics of particles inside the installation. It is clear that the kinematics of particles depends on the dynamics of the airflow. Therefore, two tasks arise here: 1) study of the dynamics of the airflow; 2) based on the obtained hydrodynamic parameters of the airflow, the study of the trajectories of the separated particles.

In practice, the bulk density of dust in separators can reach 50 g / m^3. This value is significantly lower than the density of incompressible air (1.2 kg / m^3). Therefore, in many works, the influence of the solid phase on the dynamics of air is neglected. However, near the wall where dust particles accumulate under the action of centrifugal force, the density of the solid phase can reach significant values. In this case, the influence of the solid phase on the dynamics of the gas phase cannot be neglected. Therefore, in this work, a numerical study of the turbulent flow is carried out, taking into account the influence of the solid phase on the dynamics of the airflow inside the centrifugal installation.

The modeling of three-dimensional gas flows is associated with well-known practical difficulties: the use of spaced grids, the slow convergence of a numerical solution algorithm, and a rather complicated implementation of the calculation algorithm. Solving the turbulent problem also requires thickening the calculated stack in areas with large gradients of the desired variables, as well as near solid walls. All these problems significantly complicate the physical and mathematical formulation of the problem in the field under consideration.

For a numerical study of the problem, a system of equations is used, the Reynolds averaged Navier-Stokes equations in a cylindrical coordinate system [13]:

$$\begin{cases}
\dfrac{\partial U}{\partial t}+U\dfrac{\partial U}{\partial z}+V\dfrac{\partial U}{\partial r}+\dfrac{W}{r}\dfrac{\partial U}{\partial w}+\dfrac{1}{\rho}\dfrac{\partial p}{\partial z}=\dfrac{1}{r}\dfrac{\partial}{\partial r}\left(r(\nu+\nu_t)\dfrac{\partial U}{\partial r}\right)-\sum\limits_{i=1}^{N}\dfrac{\rho_i}{\rho}k_i\left(U-U_{pi}\right); \\
\dfrac{\partial V}{\partial t}+U\dfrac{\partial V}{\partial z}+V\dfrac{\partial V}{\partial r}+\dfrac{W}{r}\dfrac{\partial V}{\partial w}-\dfrac{W^2}{r}+\dfrac{1}{\rho}\dfrac{\partial p}{\partial r}=\dfrac{1}{r}\dfrac{\partial}{\partial r}\left(r(\nu+\nu_t)\dfrac{\partial V}{\partial r}\right)-\dfrac{(\nu+\nu_t)}{r^2}V-\sum\limits_{i=1}^{N}\dfrac{\rho_i}{\rho}k_i\left(V-V_{pi}\right); \\
\dfrac{\partial W}{\partial t}+U\dfrac{\partial W}{\partial z}+V\dfrac{\partial W}{\partial r}+\dfrac{W}{r}\dfrac{\partial W}{\partial w}-\dfrac{WV}{r}=\dfrac{1}{r}\dfrac{\partial}{\partial r}\left(r(\nu+\nu_t)\dfrac{\partial W}{\partial r}\right)-\dfrac{(\nu+\nu_t)}{r^2}W-\sum\limits_{i=1}^{N}\dfrac{\rho_i}{\rho}k_i\left(W-W_{pi}\right); \\
\dfrac{\partial U_{pi}}{\partial t}+U_{pi}\dfrac{\partial U_{pi}}{\partial z}+V_{pi}\dfrac{\partial U_{pi}}{\partial r}=k_i\left(U-U_{pi}\right); \\
\dfrac{\partial V_{pi}}{\partial t}+U_{pi}\dfrac{\partial V_{pi}}{\partial z}+V_{pi}\dfrac{\partial V_{pi}}{\partial r}-\dfrac{W_{pi}^2}{r}=k_i\left(V-V_{pi}\right); \\
\dfrac{\partial W_{pi}}{\partial t}+U_{pi}\dfrac{\partial W_{pi}}{\partial z}+V_{pi}\dfrac{\partial W_{pi}}{\partial r}+\dfrac{W_{pi}V_{pi}}{r}=k_i\left(W-W_{pi}\right); \\
\dfrac{\partial \rho_i}{\partial t}+\dfrac{\partial\left(U_p\rho_i\right)}{\partial z}+\dfrac{\partial\left(V_p\rho_i\right)}{\partial r}=D\left(\dfrac{\partial^2\rho_i}{\partial r^2}+\dfrac{1}{r}\dfrac{\partial\rho_i}{\partial r}+\dfrac{\partial^2\rho_i}{\partial z^2}\right); \\
D=\dfrac{\rho}{\rho+\rho_\rho}\dfrac{\nu+\nu_t}{Sc}.
\end{cases} \tag{1}$$

The initial and boundary conditions for the system of equations (1) are set in a standard way [3]. For example, boundary conditions are set as follows:

Table 1. Fractional composition of the solid phase

Zinc particle sizes, microns	0 to 5	5 to 10	10 to 20	20 to 30	30 to 45	over 45
Source material, by weight%	16	29	35	16	4	0

For $z=0: U=U_0, V=0, W=W_0, U_{pi}=U, V_{pi}=V, W_{pi}=W$. On the walls: $U=V=W=U_{pi}=V_{pi}=W_{pi}=0$. On the axis r = 0: for $\partial\Phi/\partial r=0$, $\Phi=U$, U_{pi} and $W, V, W_{pi}, V_{pi}=0$.

In this system, U, V, W – are respectively the axial, radial, and tangential components of the airflow velocity vector; U_{pi}, V_{pi}, W_{pi} - similar components of the velocity vector for the i-th dust fraction; p– pressure; ρ is the gas density; v is its molecular viscosity; v_t is the turbulent viscosity of the airflow; ρ_ρ is the mass density of dust; k is the coefficient of interaction between air and the i-th dust fraction; N-fraction of dust fractions our work N-5; D is the diffusion coefficient for the solid phase, Sc = 0.8– Schmidt coefficient.

The coefficient of interaction between the phases is determined through the Stokes parameter:

$$k=\frac{18\rho\upsilon}{\rho_\rho\delta^2}.$$

In this expression, ρ_ρ is the density of the material of the dust particles, and δ is the "effective" particle diameter. In Table 1, the mass composition of zinc particles by size is assigned, which we divided into five fractions. System (1) is open. For closure, as mentioned above, the SARC model was used. This model belongs to the class of one-parameter turbulence models. Only one additional equation appears here for calculating the kinematic coefficient of vortex viscosity

$$\frac{\partial\rho\tilde{\nu}}{\partial t}+\nabla(\rho\tilde{\nu}U)=\rho(P_\upsilon-D_\upsilon)+\frac{1}{\sigma_\upsilon}\nabla\left[(\nu+\nu_t)\nabla\tilde{\nu}\right]+\frac{C_{b2}}{\sigma_\upsilon}\rho(\nabla\tilde{\nu})^2-\frac{1}{\sigma_\upsilon\rho}(\mu+\rho\tilde{\nu})\nabla\rho\nabla\tilde{\nu}. \tag{2}$$

Turbulent eddy viscosity is calculated from:

$$\nu_t=\tilde{\nu}f_{\upsilon 1} \tag{3}$$

The SARC model is the same as for the "standard" version (SA), except that the term P_υ is multiplied by the rotation function f_{r1} [7,11]. The remaining values remain the same as for the "standard" model, which is presented in [7].

3. Solution Methods

For the numerical implementation of the system (1), partial parabolization was performed, i.e., on the right-hand sides, the terms with derivatives with respect to z are neglected. A stream function ψ is introduced for which the continuity condition is satisfied

$$V=-\frac{1}{r}\frac{\partial\psi}{\partial z},\ U=\frac{1}{r}\frac{\partial\psi}{\partial r}. \tag{4}$$

The vorticity ζ is also introduced

$$\zeta=\frac{\partial U}{\partial r}-\frac{\partial V}{\partial z}. \tag{5}$$

Next, we exclude pressure from the first two equations of system (1) and substituting expressions (4) into (5) we obtain a system with respect to new variables.

$$\begin{cases}\frac{\partial\zeta}{\partial t}+U\frac{\partial\zeta}{\partial z}+V\frac{\partial\zeta}{\partial r}-\zeta\frac{V}{r}+\frac{1}{r^3}\frac{\partial G^2}{\partial z}=-\frac{1}{r^2}\frac{\partial}{\partial r}\left(r(\nu_{eff})\zeta\right)+\frac{1}{r}\frac{\partial^2}{\partial r^2}\left(r(\nu_{eff})\zeta\right)-\sum_{i=1}^{N}\frac{k_i}{\rho}\left(\frac{\partial}{\partial r}\left(\rho_\rho\left(U-U_{pi}\right)\right)-\frac{\partial}{\partial z}\left(\rho_\rho\left(V-V_{pi}\right)\right)\right),\\ \frac{\partial G}{\partial t}+U\frac{\partial G}{\partial z}+V\frac{\partial G}{\partial r}=\frac{1}{r}\frac{\partial}{\partial r}\left(r\upsilon_{eff}\left(\frac{1}{r}\frac{\partial G}{\partial r}-\frac{G}{r^2}\right)\right)-\frac{\nu_{eff}}{r^2}G-\sum_{i=1}^{N}\frac{k_i}{\rho}\left(\rho_\rho\left(G/r-W_{pi}\right)\right),\\ \frac{1}{r}\frac{\partial^2\psi}{\partial r^2}-\frac{1}{r^2}\frac{\partial\psi}{\partial r}+\frac{\partial^2\psi}{r\partial z^2}=\zeta,\\ \frac{\partial\tilde{\nu}}{\partial t}+U\frac{\partial\tilde{\nu}}{\partial z}+V\frac{\partial\tilde{\nu}}{\partial r}=(P_\upsilon-D_\upsilon)+\frac{1}{\sigma_\upsilon}\frac{\partial}{r\partial r}\left[r(\tilde{\nu}+\upsilon)\frac{\partial\tilde{\nu}}{\partial r}\right]+\frac{C_{b2}}{\sigma_\upsilon}\left(\frac{\partial\tilde{\nu}}{\partial r}\right)^2,\\ G=Wr,\ \upsilon_{eff}=\nu+\nu_t.\end{cases} \tag{6}$$

This system is subject to the following boundary conditions:

For z = 0: $\psi=(1-r_2^2)/2$, G = W r, $\tilde{\upsilon}=3/\mathrm{Re}$. On the wall: $\psi=(1-r_2^2)/2$, G, $\tilde{\upsilon}$ = 0. For r = 0: ψ, G, $\tilde{\upsilon}$ = 0.

The flow region is shown in Fig. 2, where R is the large radius of the annular channel; therefore, the surface of the cone corresponds to; r_1 is the radius of the inner cylinder of the first sections, r_3, r_4 is the radius of the inner cylinder of the rub and fourth sections.

For the numerical implementation of the system (6), a coordinate transformation was performed.

The first section is 0 <z <z_2.

$$\eta=\frac{\eta_0F_1(z)-F_2(z)}{F_1(z)-F_2(z)}+\frac{(1-\eta_0)r}{F_1(z)-F_2(z)};\ F_1(z)=R,\qquad F_2(z)=r_2.$$

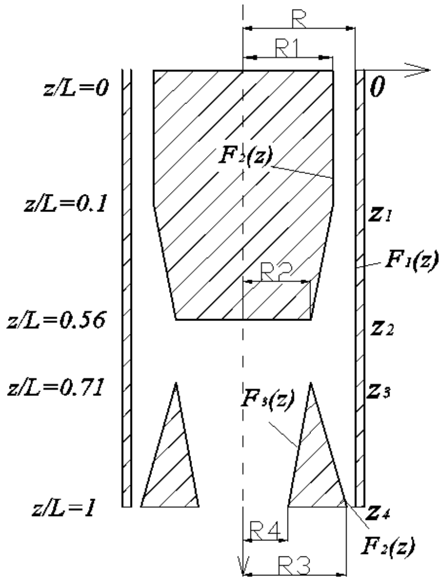

Fig. 2. The area of the separator.

The second section is $z_2 < z < z_3$.

$$\eta = \frac{r - F_2(z)}{(F_1(z) - F_2(z))}; \quad F_1(z) = R, \qquad F_2(z) = 0.$$

The third section is $z_3 < z < z_4$, $\eta < \eta_0$.

$$\eta = \eta_0 \frac{r}{F_3(z)}; \quad F_3(z) = r_2, \qquad F_2(z) = 0.$$

The fourth section is $z_3 < z < z_4$, $\eta > \eta_0$.

$$\eta = \frac{\eta_0 F_1(z) - F_2(z)}{F_1(z) - F_2(z)} + \frac{(1-\eta_0) r}{F_1(z) - F_2(z)}; \; F_1(z) = R, \qquad F_2(z) = r_4.$$

Here, F_1 *(z)* is the function of the outer cylinder, F_2 *(z)*, F_3 *(z)* is the function of the inner cylinder and cone, $\eta_0 = 0.6\eta$.

$$\begin{cases} \dfrac{\partial \zeta}{\partial t} + \dfrac{U}{L}\dfrac{\partial \zeta}{\partial \xi} + U\eta'\dfrac{\partial \zeta}{\partial \eta} + V\eta\dfrac{\partial \zeta}{\partial \eta} - \zeta\dfrac{V}{r} + \dfrac{1}{r^3 L}\dfrac{\partial G^2}{\partial \xi} + \dfrac{\eta'}{r^2}\dfrac{\partial G^2}{\partial \eta} = -\dfrac{\eta}{r^2}\dfrac{\partial\left(r(\nu_{eff})\zeta\right)}{\partial \eta} + \dfrac{\eta^2}{r}\dfrac{\partial^2\left(r(\nu_{eff})\zeta\right)}{\partial \eta^2} - \\ -\displaystyle\sum_{i=1}^{N}\dfrac{k_i}{\rho}\left(\eta\dfrac{\partial}{\partial \eta}\left(\rho_\rho\left(U - U_{pi}\right)\right) - \dfrac{\partial}{\partial \xi}\left(\rho_\rho\left(V - V_{pi}\right)\right) - \eta'\dfrac{\partial}{\partial \eta}\left(\rho_\rho\left(V - V_{pi}\right)\right)\right); \\ \dfrac{\partial G}{\partial t} + \dfrac{U}{L}\dfrac{\partial G}{\partial \xi} + U\eta'\dfrac{\partial G}{\partial \eta} + V\eta\dfrac{\partial G}{\partial \eta} = \eta\dfrac{\partial}{\partial \eta}\left((\nu_{eff})\left(\eta\dfrac{\partial G}{\partial \eta} - \dfrac{G}{r}\right)\right) - \dfrac{\nu_{eff}}{r^2}G - \displaystyle\sum_{i=1}^{N}\dfrac{k_i}{\rho}\left(\rho_\rho\left(G/r - W_{pi}\right)\right); \\ \dfrac{\eta^2}{r}\dfrac{\partial^2 \psi}{\partial \eta^2} - \dfrac{\eta}{r^2}\dfrac{\partial \psi}{\partial \eta} + \dfrac{1}{rL^2}\dfrac{\partial^2 \psi}{\partial \xi^2} + \dfrac{2\eta'}{rL}\dfrac{\partial^2 \psi}{\partial \xi \partial \eta} + (\eta')^2\dfrac{\partial^2 \psi}{r\partial \eta^2} + \eta''\dfrac{\partial \psi}{r\partial \eta} = \zeta, \\ \dfrac{\partial U_{pi}}{\partial t} + U_{pi}\dfrac{\partial U_{pi}}{\partial \xi} + U_{pi}\eta'\dfrac{\partial U_{pi}}{\partial \eta} + V_{pi}\eta\dfrac{\partial U_{pi}}{\partial \eta} = k\left(U - U_{pi}\right); \\ \dfrac{\partial V_{pi}}{\partial t} + U_{pi}\dfrac{\partial V_{pi}}{\partial \xi} + U_{pi}\eta'\dfrac{\partial V_{pi}}{\partial \eta} + V_{pi}\eta\dfrac{\partial V_{pi}}{\partial \eta} = k\left(V - V_{pi}\right); \\ \dfrac{\partial \rho_\rho}{\partial t} + \dfrac{\partial\left(U_{pi}\rho_\rho\right)}{\partial \xi} + \eta'\dfrac{\partial\left(U_{pi}\rho_\rho\right)}{\partial \eta} + \eta\dfrac{\partial\left(V_{pi}\rho_\rho\right)}{\partial \eta} = D\left(\eta^2\dfrac{\partial^2 \rho_\rho}{\partial \eta^2} + \dfrac{\eta}{r}\dfrac{\partial \rho_\rho}{\partial \eta} + \dfrac{\partial^2 \rho_\rho}{\partial \xi^2} + 2\eta'\dfrac{\partial^2 \rho_\rho}{\partial \zeta \partial \eta} + (\eta')^2\dfrac{\partial^2 \rho_\rho}{\partial \eta^2} + \eta''\dfrac{\partial \rho_\rho}{\partial \eta}\right) \\ \dfrac{\partial \tilde{\upsilon}}{\partial t} + U\dfrac{\partial \tilde{\upsilon}}{\partial \xi} + U\eta'\dfrac{\partial \tilde{\upsilon}}{\partial \eta} + V\eta\dfrac{\partial \tilde{\upsilon}}{\partial \eta} = (P\upsilon - D\upsilon) + \dfrac{\eta}{r\sigma_\upsilon}\dfrac{\partial}{\partial \eta}\left[r(\tilde{\upsilon} + \upsilon)\eta\dfrac{\partial \tilde{\upsilon}}{\partial \eta}\right] + \dfrac{C_{b2}}{\sigma_\upsilon}\left(\eta\dfrac{\partial \tilde{\upsilon}}{\partial \eta}\right)^2. \end{cases} \tag{7}$$

The following boundary conditions were set for the problem: on the wall, i.e., all speeds will be zero, and on the wasps $\partial\Phi / \partial r = 0$ for $\Phi = U, \upsilon$ and $W, V = 0$. To start the calculation, we set the values $\nu = 3 / Re$, at the output - the Neumann condition was set to the Reynolds number depending on the input flow rate.

Thus, the new variables make it possible to bring all the equations of the system to a parabolic form and this system can be written in vector form

$$\frac{\partial \Phi}{\partial t} + U\frac{\partial \Phi}{\partial x} + V\frac{\partial \Phi}{\partial y} = \nu\frac{\partial^2 \Phi}{\partial y^2}. \tag{8a}$$

In this equation:

$$\Phi = \begin{bmatrix} \zeta \\ G \\ \tilde{\nu} \end{bmatrix}$$

$$\frac{\Phi_{i,j}^{n+1} - \Phi_{i,j}^{n}}{\Delta t} + 0.5\cdot(U + |U|)\frac{\Phi_{i,j}^{n} - \Phi_{i-1,j}^{n}}{\Delta \xi} + 0.5\cdot(U - |U|)\frac{\Phi_{i,j+1}^{n} - \Phi_{i,j}^{n}}{\Delta \xi} + 0.5\cdot(V + |V|)\frac{\Phi_{i,j}^{n} - \Phi_{i,j-1}^{n}}{\Delta \eta} + 0.5\cdot(V - |V|)\frac{\Phi_{i,j+1}^{n} - \Phi_{i,j}^{n}}{\Delta \eta} = \nu\frac{\Phi_{i,j+1}^{n} - 2\Phi_{i,j}^{n} + \Phi_{i,j-1}^{n}}{\Delta \eta^2}. \tag{8b}$$

For the numerical implementation of ζ, G, and ν in equations (8), an implicit scheme was used. It is absolutely stable, and the unknowns on a new layer were swapped. The integration steps were $\Delta\xi = 0.05$, $\Delta\eta = 0.02$. The number of calculation points in the transverse direction was 50; the longitudinal direction was 100. Such a grid is very suitable for engineering tasks. To ensure stability in the numerical solution of system (8), a different scheme against the flow was used, and the diffusion terms were approximated by a central difference.

The Poisson equation for the stream function was also approximated by the central difference, and the iteration method of upper relaxation was used to resolve it.

$$\frac{\psi^{k}{}_{i+1,j} - 2\psi^{k+1}{}_{i,j} + \psi^{k}{}_{i-1,j}}{\Delta \xi^2} + \frac{\psi^{k}{}_{i,j+1} - \psi^{k}{}_{i,j-1}}{2\Delta \eta} + \frac{\psi^{k}{}_{i+1,j+1} - \psi^{k}{}_{i-1,j+1} + \psi^{k}{}_{i+1,j-1} - \psi^{k}{}_{i-1,j-1}}{2\Delta\xi\Delta\eta} + \frac{\psi^{k}{}_{i,j+1} - 2\psi^{k+1}{}_{i,j} + \psi^{k}{}_{i,j-1}}{\Delta \eta^2} = r_j \zeta_{i,j}^{k}. \tag{9}$$

The initial and boundary conditions for the equations in the SARC model are set in a standard way, which are discussed in detail in [7,11]. As mentioned above, the Lagrange approach is convenient for calculating particle trajectories. For this purpose, we write 3-5 equations in system (7) in the form

$$\begin{cases} \dfrac{dU_{pi}}{dt} = k_i\left(U - U_{pi}\right), \\ \dfrac{dV_{pi}}{dt} = k_i\left(V - V_{pi}\right), \\ \dfrac{dW_{pi}}{dt} = k_i\left(W - W_{pi}\right). \end{cases} \tag{10}$$

In this system, the derivative in the right-hand sides of the equations is the substantial derivative

$$\frac{d}{dt} = \frac{\partial}{\partial t} + U_{pi}\frac{\partial}{\partial \xi} + U_{pi}\eta'\frac{\partial}{\partial \eta} + V_{pi}F(z)\frac{\partial}{\partial \eta} \tag{11}$$

For the numerical implementation of U_{pi}, V_{pi}, W_{pi} in equations (7), an implicit scheme was used.

$$\Phi = \begin{bmatrix} U_{pi} \\ V_{pi} \\ W_{pi} \end{bmatrix},$$

$$\frac{\Phi_{i,j}^{n+1} - \Phi_{i,j}^{n}}{\Delta t} + 0.5(U_{pi} + |U_{pi}|)\frac{\Phi_{i,j}^{n} - \Phi_{i-1,j}^{n}}{\Delta \xi} + 0.5(U_{pi} - |U_{pi}|)\frac{\Phi_{i,j+1}^{n} - \Phi_{i,j}^{n}}{\Delta \xi} + 0.5(V_{pi} + |V_{pi}|)\frac{\Phi_{i,j}^{n} - \Phi_{i,j-1}^{n}}{\Delta \eta} + 0.5(V_{pi} - |V_{pi}|)\frac{\Phi_{i,j+1}^{n} - \Phi_{i,j}^{n}}{\Delta \eta} = k\left(U - \Phi_{i,j}^{n+1}\right). \tag{12}$$

It is absolutely stable, and unknown on a new layer which was run by. After the formation of the quasi-periodic regime, unsteady fields were averaged. The parameters of the laboratory installation of the separator had the following values: $L=650$ *mm*, $R=125$ *mm*, $r_1=100$ *mm*, $r_2=75$ *mm*, $r_3=120$ *mm*, $r_4=50$ *mm*. The experiments were carried out with the following values of the flow parameters at the entrance to the coaxial channel: $U_{ref} = U_0$, $W_{ref} / U_{ref} = 0.5$, and $W_{ref}/ U_{ref}= 2$. $\rho^0 = 7000 kg / m^3$. The total density of the solid phase at the inlet was $\sum_{i=1}^{N}\rho_i = 18\ g / m^3$ and was uniformly distributed over the cross section.

4. Discussion of the Results

Figure 3 illustrates air velocity profiles in section $\xi = 0.65$. Here U / U_{ref}, V / V_{ref}, W / W_{ref} are dimensionless speeds. Here, $U_{ref}= U_0$, $W_{ref}/U_{ref} = 0.5$ and $W_{ref} / U_{ref} = 2$.

The numerical results show that with an increase in the initial swirl of the flow, the influence of the solid phase on the dynamics of the airflow also increases. This effect is explained by the fact that with strong swirls due to centrifugal force, the concentration of the solid phase near the wall of the air separator body increases significantly, which also leads to an increase in the effect on the dynamics of air.

A dispersion analysis of the powder was carried out by a MALVERN laser analyzer. To compare the results of numerical calculation with experimental data, a dispersed analysis of dust from a hopper separator was performed, i.e., dust collected by a centrifugal separator. Figure 4 shows the dispersed composition of dust from the separator hopper according to the analyzer (diamond points) for $U_0 = 9.5 m / c$, and according to the numerical calculation according to the above model, the solid line taking into account the influence of the solid phase on the airflow dynamics dashed without taking into account the influence of the solid phase on the airflow dynamics at $W_{ref} / U_{ref} = 2$.

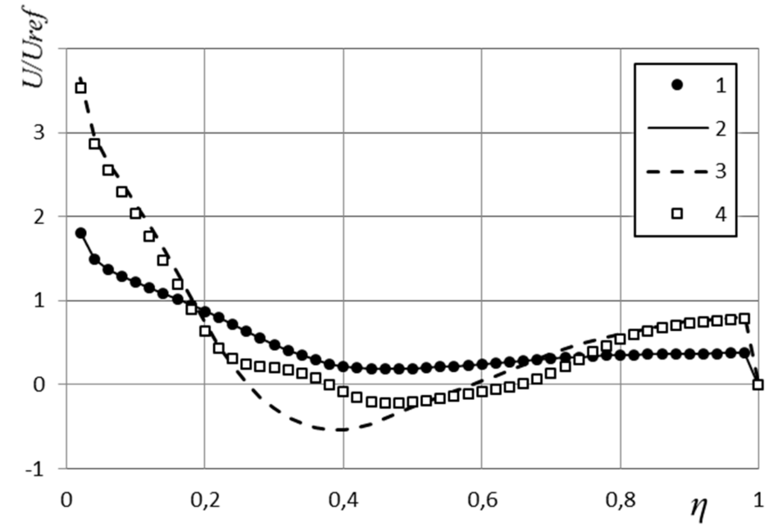

(a)

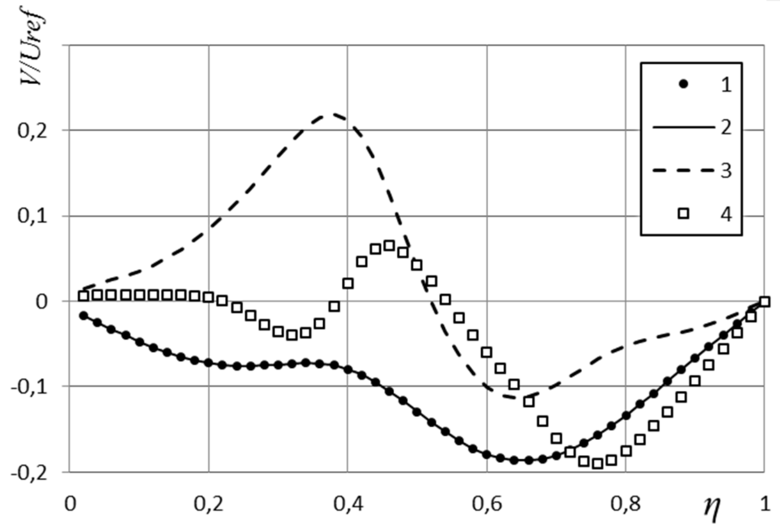

(b)

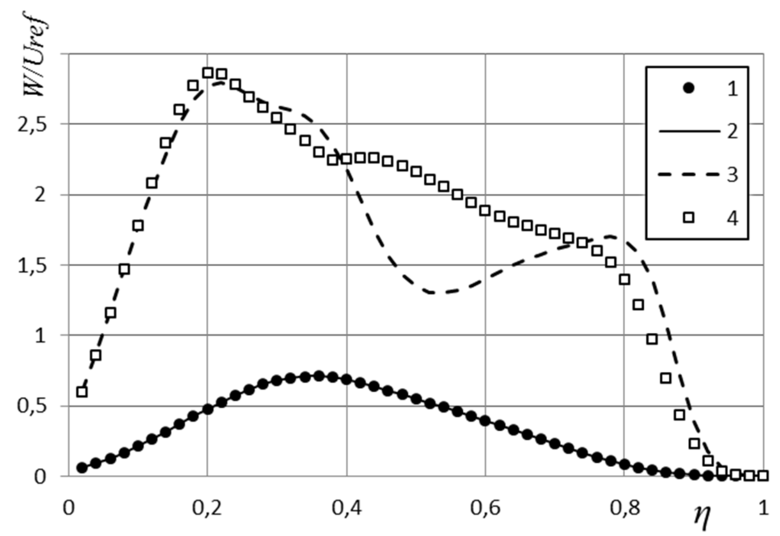

(c)

Fig. 3. Profiles a) axial, b) radial, and c) tangential air velocity in the section $\xi = 0.65$. 1-taking into account the effect of the solid phase on the airflow at $W_{ref} / U_{ref} = 0.5$, 2-without taking into account the effect of the solid phase on the airflow at $W_{ref} / U_{ref} = 0.5$, 3-taking into account the effect of the solid phase on the airflow at $W_{ref} / U_{ref} = 2$, 4-without taking into account the influence of the solid phase on the airflow at $W_{ref} / U_{ref} = 2$.

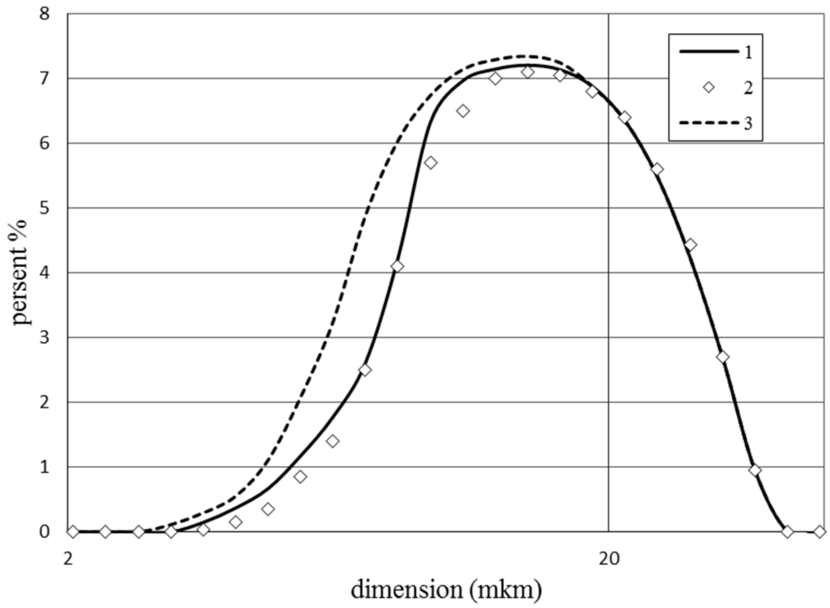

Fig. 4. Dispersion analysis of the composition of dust from the hopper separator. 1-taking into account the influence of the solid phase on the dynamics of the airflow, 2-experiment, 3-without taking into account the influence of the solid phase on the dynamics of the airflow.

The numerical results from (Fig. 4) the SARC turbulence model at $W_{ref} / U_{ref} = 2$ shows an accuracy of 86% when taking into account the influence of the solid phase on the dynamics of the airflow, 79% without taking into account the effect of the solid phase on the dynamics of the air stream.

5. Conclusions

A mathematical model was developed for calculating the hydrodynamics of a swirling turbulent flow occurring in an air-centrifugal separator. The primary laws of such a course were revealed. The presented mathematical model allowed not only to study the complex picture of the swirling turbulent flow, which contributes to the development of new promising methods for the classification of powders but also to optimize the operating and geometric parameters of existing plants. It was shown in the paper that the SARC turbulence model adequately describes the swirling flow inside a centrifugal separator.

Conflict of Interest

The author declared no potential conflicts of interest with respect to the research, authorship and publication of this article.

Funding

The author received no financial support for the research, authorship, and publication of this article.

Nomenclature

υ	Molecular viscosity	ψ	Stream function
υ_t	Turbulent viscosity	ζ	Vorticity
$\tilde{\upsilon}$	Turbulent eddy viscosity [1/s^2]	t	Time [s]
U_{pi}, V_{pi}, W_{pi}	Similar components of the velocity vector for the i-th dust fraction	x	Length [m]

References

[1] Gupta, A.K., Lilly, D.G., Syred, N., *Swirl Flows*, In: Swirl flows. Kent Engl: Abacus, 1984.
[2] Muntean, S., Susan-Resiga, R.F., Bosioc, A.I., Proc. 3th IAHR International Meeting of the Workgroup on Cavitation and Dynamic Problems in Hydraulic Machinery and Systems, October 14–16, Brno, Czech Republic, 2009.
[3] Okulov, V.L., Sorensen, J.N., Maximum efficiency of wind turbine rotors using Joukowsky and Betz approaches, *Journal of Fluid Mechanics,* 649, 2010, 497-508.
[4] Syred, N.A., Review of oscillation mechanisms and the role of the processing vortex core (PVC) in swirl combustion systems, *Prog. Energy Combust. Sc.*, 32(2), 2006, 93–161.
[5] Derksen, J.J., Separation performance predictions of a Steinman high-efficiency cyclone, *AIChE J.,* 49(6), 2003, 1359–1371.
[6] Shilyaev, M.I., Shilyaev, A.M., Modeling the process of dust collection in a once-through cyclone. 2. Calculation of the fractional slip coefficient, *Thermophysics and Aeromechanics,* 10(3), 2003, 427–437.
[7] Spalart, P.R., Shur, M.L., On the sensitization of turbulence models to rotational and curvature, *Aerospace Science and Technology,* 1(5), 1997, 297-302.
[8] Spalart, P.R., Allmaras, S.R., A one-equation turbulence model for aerodynamic flow, *AIAA*, 12, 1992, 439–478.
[9] Steenburgen, W., *Turbulent pipe flow with swirl*, PhD Thesis, Eindhoven University of Technology, The Netherlands, 1995.
[10] Bradshaw, P., Ferriss, D.H., Atwell, N.P., Calculation of boundary layer development using the turbulent energy equation, *J. Fluid Mech.*, 28, 1967, 593-616.
[11] Shur, M.L, Strelets, M.K, Travin, A.K, Spalart, P.R., Modeling of turbulence in rotating and curved channels: estimation of Spalart-Shur correction, *AIAA Journal,* 38(5), 2000, 784-792.
[12] Launder, B.E., Spalding, D.B., *Lectures in Mathematical Models of Turbulence*, Academic Press, London, 1972.
[13] Nigmatulin, R.I., *Dynamics of multiphase media,* CRC Press; 1st edition, 1990.

ORCID iD

Madaliev Murodil Erkinjon son https://orcid.org/0000-0001-9994-8907

How to cite this article: Erkinjon son M.M. Numerical Calculation of an Air Centrifugal Separator Based on the SARC Turbulence Model, *J. Appl. Comput. Mech.*, 6(SI), 2020, 1133–1140. https://doi.org/10.22055/JACM.2020.31423.1871